Geophysical Prospecting, 1994, 42, 953–974

Inversion for seismic anisotropy using genetic algorithms[1]

Steve Horne[2, 3] and Colin MacBeth[2]

Abstract

A general inversion scheme based on a genetic algorithm is developed to invert seismic observations for anisotropic parameters. The technique is applied to the inversion of shear-wave observations from two azimuthal VSP data sets from the Conoco test site in Oklahoma. Horizontal polarizations and time-delays are inverted for hexagonal and orthorhombic symmetries. The model solutions are consistent with previous studies using trial and error matching of full waveform synthetics. The shear-wave splitting observations suggest the presence of a shear-wave line singularity and are consistent with a dipping fracture system which is known to exist at the test site. Application of the inversion scheme prior to full waveform modelling demonstrates that a considerable saving in time is possible whilst retaining the same degree of accuracy.

Introduction

For an anisotropic material, the shear-wave phase velocity surface is no longer represented as a single continuous sheet, as is the case for isotropic materials, but as two separate sheets which may touch or intersect at singularities. Therefore, in anisotropic materials it is generally the case that three body waves may propagate: these are the quasi-compressional (qP) and the faster ($qS1$) and the slower quasi ($qS2$) shear waves each of which propagate with polarizations and velocities fixed

[1] Received February 1994, revision accepted July 1994.

[2] Edinburgh Anisotropy Project, British Geological Survey, Murchison House, West Mains Road, Edinburgh, EH9 3LA, Scotland, U.K.

[3] Department of Geology and Geophysics, University of Edinburgh, West Mains Road, Edinburgh, Scotland, U.K.

by the direction of propagation. A seismic source may therefore excite two shear waves and a qP wave each with distinct polarizations and velocities. These continue to propagate through the medium leading to a time-delay between the fast and the slow shear waves, this phenomenon is known as shear-wave splitting. The $qS2$–$qS1$ time-delay is proportional to the distance travelled through the anisotropic medium, inversely proportional to the shear-wave velocity anisotropy, and is therefore a cumulative measure of the anisotropy sampled along the raypath. The recorded shear-wave polarizations depend on the relative amounts of anisotropy sampled along the raypath. Complications can arise if the split shear waves impinge on another different anisotropic region since further splitting may occur producing a wave train that is difficult to interpret. Shear-wave splitting is commonly measured in terms of the time-delay between the split shear waves and the polarization direction of the $qS1$ arrival, since other quantities such as the differential shear-wave attenuation are difficult to estimate from field records although processing techniques have been developed which permit such measurements.

Intrinsically anisotropic materials are not thought to be the most common cause of observed anisotropy in the earth. One alternative explanation for seismic anisotropy is presented by the effective averaging that occurs when finely-layered isotropic materials are sampled by seismic energy with wavelengths greater than the thickness of the layers (Backus 1962; Folstad and Schoenberg 1993). In most cases where the layering is sub-horizontal, the resultant symmetry is transversely isotropic with a vertical (TIV) axis of symmetry (azimuthally isotropic). Aligned fractures and cracks embedded in an isotropic solid can also produce an effective anisotropic medium, which for vertical cracks gives a transversely isotropic medium with a horizontal (TIH) axis of symmetry (azimuthally anisotropic). It is possible that an effectively anisotropic medium may be produced by a combination of aligned cracks embedded in a fine layering sequence, such a symmetry system is orthorhombic if the cracks are orthogonal to the bedding planes or monoclinic, otherwise. It is useful to be able to know the symmetry, orientation and degree of these equivalent anisotropic media as this helps to identify the underlying physical cause. This knowledge is of value in resolving the heterogeneities which control the characteristics of the reservoir.

Inversion schemes for shear-wave anisotropy have been largely neglected due to the non-linearity of the problem. Chapman and Pratt (1992) suggested that the mean shear-wave arrival times could be inverted for a weak anisotropic medium by using degenerate perturbation theory to linearize the problem. Arts, Helbig and Rasolofosaon (1991) have used a localized inversion scheme based on a gradient method to invert for phase velocity measurements from laboratory experiments. However, the anisotropic model space is probably multi-modal and the- use of a gradient-based technique is likely to be very dependent on the initial model. MacBeth (1991) attempted to invert shear-wave observations using a systematic search of a precalculated database of shear-wave attributes corresponding to the discretized anisotropic model space. The drawback to this type of approach is the

necessity of constructing the database prior to the inversion. For realistic model spaces this becomes computationally impractical because of the massive initial calculations required, subsequent storage of the database and access speeds to the database during the search. What is required is an efficient search mechanism which can be applied to very large, multimodal, non-linear model spaces. A solution to this problem is offered by genetic algorithms which may be considered an efficient directed Monte Carlo search.

Genetic algorithms

Genetic algorithms (GA), which are thought to be non-linear global optimization schemes (Goldberg 1989), are receiving increasing attention due to their robustness, efficiency and suitability to many different problem domains (Stoffa and Sen 1991; Smith, Scales and Fischer 1992; Sambridge and Drijkoningen 1992). GAs can be classed alongside simulated annealing, since-both are considered as directed searches guided by random processes and both attempt to model natural processes. In the case of simulated annealing the scheme mimics the energy minimization process that accompanies crystallization, whilst GAs attempt to simulate evolution. GAs achieve this by using genetic operations to manipulate individuals (chromosomes), each representing a model, and the set of these define a population. The operators are applied to the current population so that a new population is created with new individuals which, on average, are 'fitter', that is, nearer the optimal solution. The crucial factor underlying the GA's operation lies in the coding of model parameters in the chromosome. It is these codings that the GA manipulates in the optimization process by a passive search for similarities in the 'more' successful models, known as schemata. There are many choices available for the coding but the usual choice for the representation is a single string (haploid) with individual parameters linearly mapped to binary substrings which are then concatenated. For example, a model could be represented by the following coding, 0011 |001| 1000 |000, where the vertical bar indicates a partition between adjacent parameters and is not a feature of the coding. If this is coded so that the most significant bit is to the left of each partition then the coding represents the values 3 |1|8 |0. These would then map directly to the actual model parameter values. Thus each model in the population is represented as a binary string. The simplest implementation of a GA uses only three genetic operations (the crossover and mutation operators are shown schematically in Fig. 1).

1. Reproduction: Two models are selected at random from the current population, with a probability proportional to the quantity being optimized.
2. Crossover: The models exchange portions of their codings at a point selected at random along the length of the string. This operator is applied with a fixed probability, P_c, to the two models selected by the reproduction step.

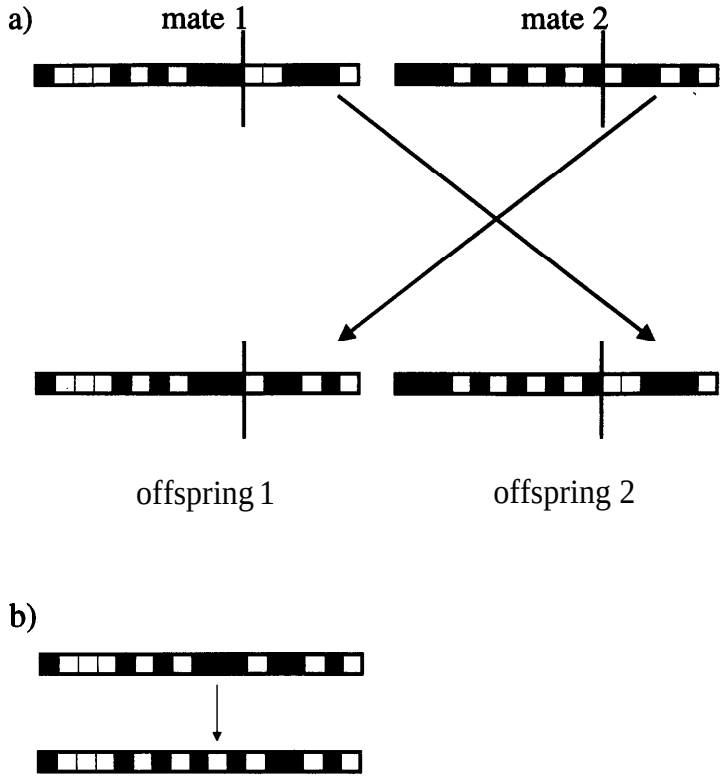

Figure **1. A schematic illustration of the operators employed by the genetic algorithm. The lines of black and white boxes represent a binary coding of a single model in the population. The crossover operator is illustrated in (a) where the two parent strings previously selected in the reproduction step exchange parts of their coding to produce two new offspring. In (b) the mutation operator is shown operating on a single bit in a models binary representation selected at random.**

3. Mutation: A single bit is selected at random along the string and its value changed. This is a background operation applied with a small fixed probability, P_m, and is included to prevent the permanent loss of any genetic information.

A schematic illustration of a GA operation is shown in Fig. 2 in comparison to other commonly used optimization techniques. The first frame of Fig. 2a shows the initially random distribution of solutions in a 2D model space corresponding to the initial population of models. As the genetic operators are applied, the model distribution becomes denser around both the local and global optima although some solutions still occupy 'poor' regions, as shown in the second and third frames of Fig. 2a. The last frame of Fig. 2a shows the final population with most solutions clustered around the global optimum with several solutions approaching the optimal value. The behaviour of a simpler Monte Carlo search is shown in Fig. 2b and it can be seen that within each frame the models are randomly distributed over the entire model space. A local gradient technique is illustrated in Fig. 2c with four initial solutions chosen randomly as shown in the first frame converging in the final frame to three local minima and the global optimum. The potential disadvantage in using GAs is that many models need to be evaluated before convergence and their

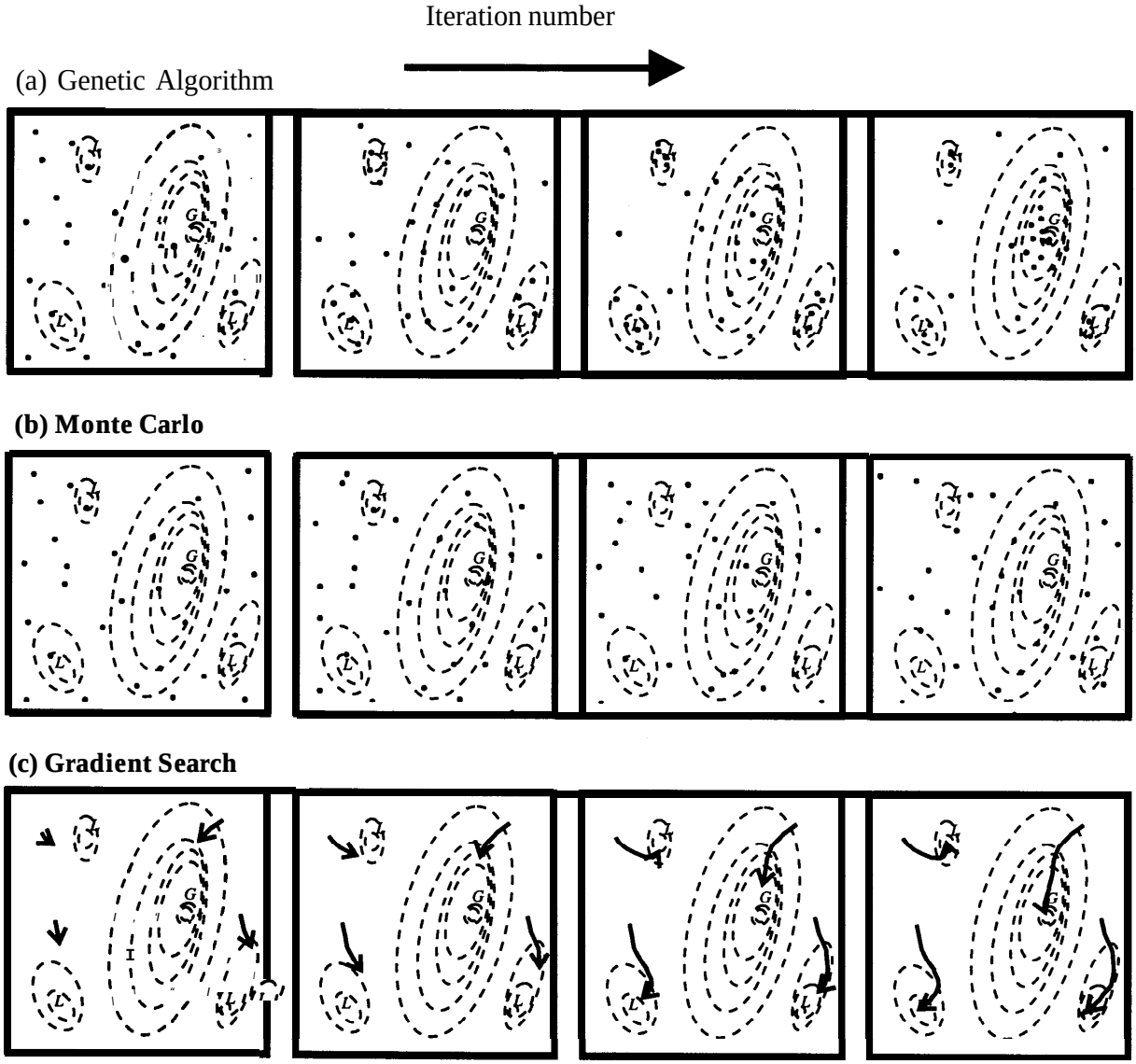

Figure **2. Schematic illustration of (a) a GA, (b) simple Monte Carlo and (c) local gradient searches for the optimization of a multimodal function in two dimensions during the** interation **of the various methods. The Ls denote local optima and Gs the global optimum. For** (a) **and (b) the black dots indicate solutions sampled by the algorithms and for (c) the arrowed paths indicate the search directions from various starting** models.

use may not be practical for problems where the forward modelling requirement is computationally expensive. As a further indication of a GA performance we show convergence curves in Fig. 3 for both a GA and a Monte Carlo search applied in a minimization role for synthetic data. This diagram shows behaviour typical of a GA with most of the minimization occurring at the beginning of the GA operation.

Our implementation of a GA is based on the three basic operations of reproduction, crossover and mutation but we also include more advanced methods (such as sharing and 'inversion' which is described in detail by Goldberg (1989)). Also included is a local search operator based on a steepest gradient method so that our

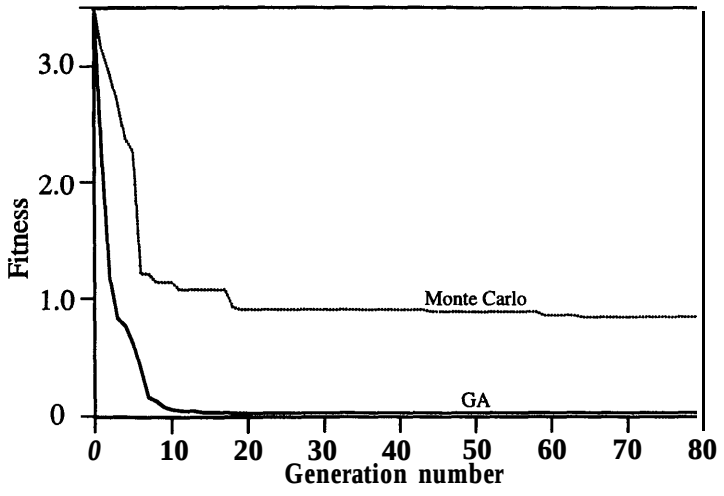

Figure **3. Comparison of a GA inversion scheme and a simple Monte Carlo search for seismic anisotropic parameters applied to synthetic data. The convergence of the GA and Monte Carlo searches are shown as solid and dotted lines, respectively.**

scheme is a hybrid of both global and local search strategies. This has the advantage that the global search performed by the GA is enhanced by the local search to improve convergent behaviour.

Application of the genetic algorithm to seismic anisotropic inversion

Most inversion schemes dealing with seismic anisotropy have concentrated on the inversion of *qP*-wave travel-times. This is because the *qP*-wave velocity sheet does not exhibit any singular behaviour so that linearization can be readily applied (Chapman and Pratt 1992). Shear-wave surveys have been largely neglected because the associated technology of multicomponent geophones and shear-wave sources are only a relatively recent advance in seismology and an understanding of their utility in the exploration and production industry is still developing (Tatham and McCormack 1991). Aside from the practical problems of obtaining estimates of the shear-wave attributes from the seismic traces is the inversion itself. Unlike the *qP*-wave velocity, the shear-wave velocities cannot be conveniently linearized owing to kiss, line and point singularities and the deviation of the group and phase velocity surfaces. However, it has been suggested that it is the shear waves that are most sensitive to the anisotropy caused by aligned thin cracks and consequently reveal more information on crack and fracture parameters than *qP*-wave observations (Crampin 1985).

The anisotropic model space can be parametrized using several different representations such as the elastic constants, the anisotropic parameters of Thomsen (1986), or parameters defining aligned isolated micro-cracks (Hudson 1991). The parametrization chosen for this inversion is the long wavelength equivalent medium for microcracks formulated by Hudson (1986) since these allow a physically intuitive interpretation for the anisotropy, which is not readily obtained from

the inspection of elastic constants. The disadvantage of this approach is that the elastic constants are restricted to the anisotropic systems defined by this model. The model consists of a single homogeneous layer with an embedded fracture system which can be represented as an equivalent anisotropic system. The model space for a single set of sub-vertical cracks is parametrized in terms of five parameters, the first three of these defining the crack properties and the remaining two the orientation of the crack system.

1. Crack Density (CD,): This is a dimensionless quantity defined by the following equation

$$CD, = \frac{N\langle a^3 \rangle}{V},$$

where N is the number of cracks in a volume v and $\langle a^3 \rangle$ is the average of the crack radius cubed. A ***CD,*** of zero implies an isotropic solid. ***CD,*** ranges from 0.0 to 0.15 in 32 increments giving a five-bit string.

2. Aspect Ratio (AR,): The ratio of the crack thickness to its diameter. AR, ranges from 0.001 to 0.3 in 32 increments, again giving a five-bit string.

3. Content (CT,): The content of the cracks is either wet (water-filled) or dry (gas-filled), represented by a single bit.

4. Direction of the crack strike in the horizontal plane (*AZI*) ranging from 0 to 180" in 64 increments, giving a string length of 6 bits.

5. Direction of the crack dip measured from the vertical axis ***(DIP)*** ranging from $-32°$ to + 32" in 32 increments, again giving a five-bit string.

The anisotropy is calculated for microcracks originally vertical and aligned along the horizontal y-axis (we use a right-handed co-ordinate system with z down and x pointing north). The system is then subjected to a rotation in the vertical $x - z$ plane about the y-axis by an angle ***DIP,*** followed by rotation by an angle *AZI* in the horizontal $x -$ y plane about the z-axis. On both the CD_1 and AR, parameters, upper limits of 0.15 and 0.3 must be imposed, respectively (Douma 1988), due to the limitations of Hudson's theory. For zero dip the cracks are vertically oriented with the direction of the symmetry axis given by the *AZI* parameter; such a system is TIH. Horizontally oriented cracks with a dip of 90" give rise to a TIV medium. For the inversion of orthorhombic symmetry, a second set of crack parameters is introduced which are orthogonal to the first set. This second crack set may model the effect of fine-layering. This gives an extra three parameters of ***CD,,*** AR_2 and CT,, with these cracks initially constrained to lie in the horizontal plane and then this combined dual crack system is rotated as before. Inversions for a hexagonal system with a horizontal symmetry axis requires a string of length 17 bits, an arbitrarily oriented symmetry axis requires 22 bits, and an arbitrarily oriented orthorhombic system requires 33 bits.

The forward modelling requirement is to calculate a set of predictions for the shear-wave attributes corresponding to any of the crack models (chromosomes) in

the population. To do this we compute the corresponding elastic constants for these crack parameters, and the phase velocities and polarizations for a range of propagation directions using the Kelvin-Christoffel equation (Musgrave 1970). These phase velocities and polarizations are then used to construct the corresponding group velocities and polarizations. This can be achieved by constructing a wave surface, equivalent to the group-velocity surface, derived from the envelope of wavefronts (Musgrave 1970). It is important to use these group, rather than the phase, attributes since it is these quantities that are observed. In practice only a quadrant of up- or down-going waves need to be calculated for orthorhombic or higher symmetry systems, since the remaining directional variations can be found by exploiting mirror symmetries.

Once the predicted group velocities and polarizations have been calculated, a misfit function between the predicted and observed estimates can be calculated. This misfit function takes the form

$$f(\mathbf{M}, \boldsymbol{\tau}^0, \boldsymbol{p}^0) = \frac{1}{2N}\left(\sum_{i=1}^{N} \frac{(\tau_i^0 - \tau_i^m)^2}{\delta\tau_i^2}\right)^{1/2} + \frac{1}{2N}\left(\sum_{i=1}^{N} \frac{(p_i^0 - p_i^m)^2}{\delta p_i^2}\right)^{1/2},$$

where τ_i^0 is a component of the vector of the observed $qS2 - qS1$ time-delays, τ_i^m is a component of the vector of model estimates for the $qS2 - qS1$ time-delay. Similarly p_i^0 is a component of the vector of the observed $qS1$-wave polarization, p_i^m is a component of the vector of model estimates for $qS1$-wave polarization. $\delta\tau_i$ and δp_i are the estimated errors for the ith observation for the time-delays and the $qS1$-wave polarizations respectively. The summations are over the number of polarization and time-delay observations N. Each observation i represents a raypath from source to receiver. More specifically, the vector of model parameters M is a set of crack and orientation values corresponding to one of the chromosomes in the GA's population. A misfit value of less than one implies that all observations are, on average, within the estimated errors. The GA is then applied in the minimization of the least-squares misfit function between the predictions and the observed estimates. The typical CPU time required for convergence is approximately 40 minutes on a VAX 4000/400 (Specmark 22.3).

Application to field data sets

Experimental configuration for azimuthal VSP (A VSP)

An example of the inversion procedure is presented here from an azimuthal VSP (AVSP) shot by Conoco in 1986, at the Conoco Borehole Test Facility (CBTF), Kay County, Oklahoma. The results from this survey have been previously published (Queen and Rizer 1990) as part of an extensive study of the natural fracturing occurring at the site. The AVSP was one of a number of experiments including surface fracture mapping, point load tests on oriented core samples, dip-

meter data and borehole televiewers (BHTV), which attempted to characterize the fractures at the CBTF.

The geology of the test site is sufficiently simple to neglect any significant ray bending or complications due to irregular interfaces. Ray tracing through a velocity structure derived from sonic logs indicates that the rays follow an essentially straight line between the source and receiver (Fig. 4) with no critical refractions lying outside the internal shear-wave window as defined by Liu and Crampin (1990). This study is useful because of the abundance of diverse and independent fracture-related information allowing verification of any hypothesis relating seismic anisotropy to cracks or fractures, such as that proposed by Crampin (1987). The AVSP consisted of nine shotpoints surveyed at 15" intervals lying on an offset arc of radius 290 m about well 33-l (Fig. 5). Recordings were made using a three-component sonde at five levels with the shallowest at a depth of 582 m and equi-spaced at 10 m intervals thereafter. In-line and cross-line shear and compressional vibroseis sweeps were used in the experiment with frequency sweeps from 7 to 46 Hz and 18 to 96 Hz for the shear and compressional vibrators, respectively.

Processing and wavefield parametrization

After conventional seismic processing of the data, which includes cross-correlation, stacking and correction for sonde rotation using gyro data, two automatic estimation techniques, the dual-source cumulative technique (DCT) (Zeng and MacBeth

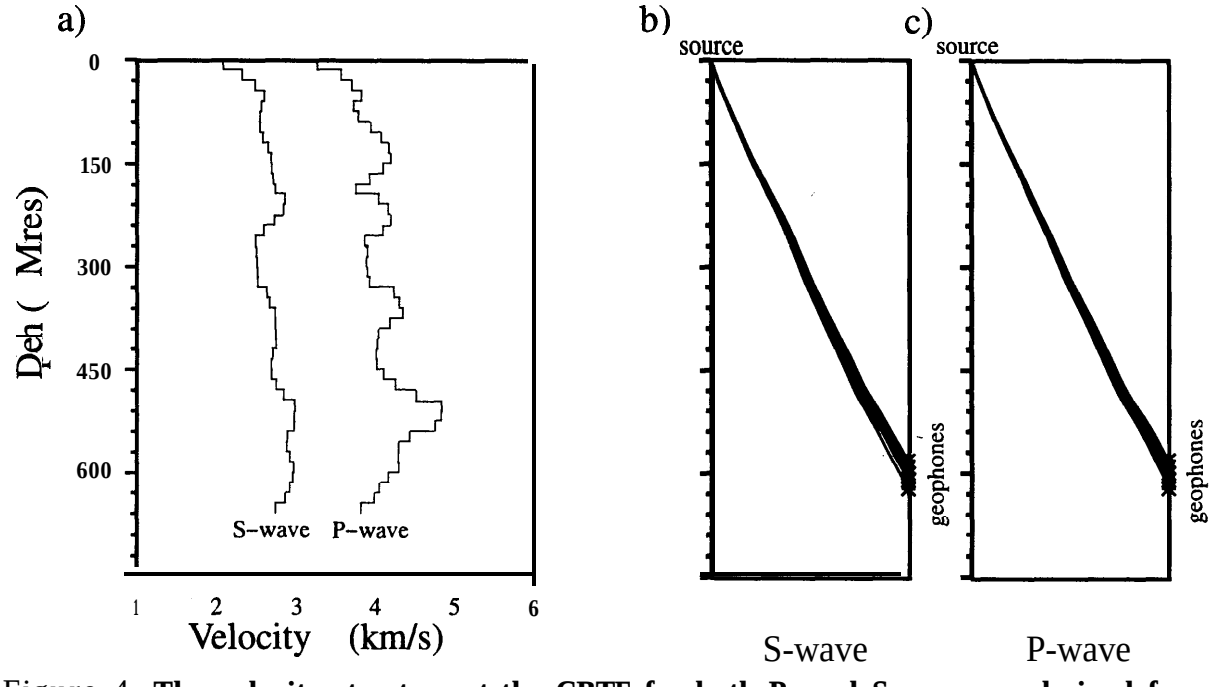

Figure 4. **The velocity structure at the CBTF for both P- and S-waves as derived from sonic logs obtained in well 33-l. Isotropic ray tracing for both P- and shear-waves are shown in (b) and (c) for source and geophone positions corresponding to the azimuthal VSP geometry.**

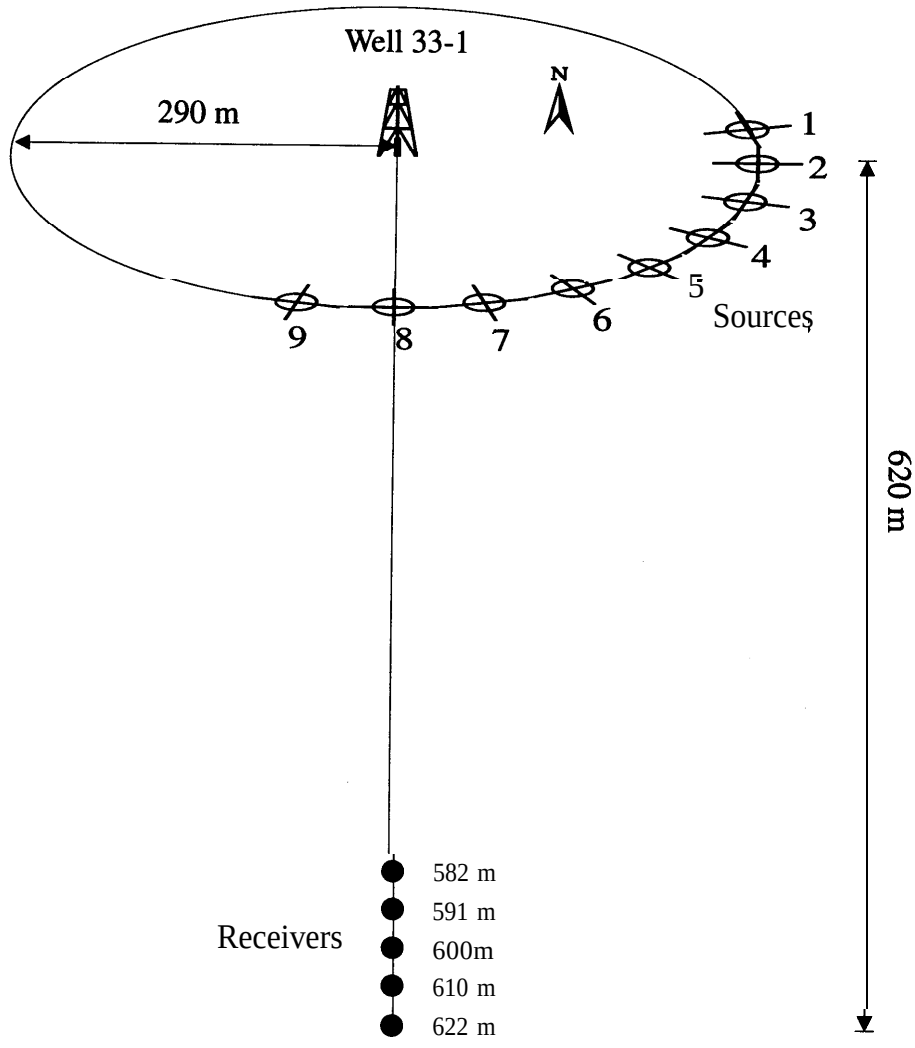

Figure **5. Schematic illustration of the acquisition geometry used for the azimuthal VSP showing the vibroseis source positions, as indicated by the crossed circles, and the three-component geophone positions indicated by the filled circles.**

1993) and the linear transform technique (LTT) (Li and Crampin 1993), were applied to the shear-wave traces in order to estimate the $qS1$-wave polarization direction and the $qS2 - qS1$ time-delay. These results agree with those published by Queen and Rizer (1990) which were obtained using a numerical rotation analysis (Alford 1986), suggesting a consistent processing sequence. The lateral uniformity of the geology around the test site and the constant source offset reduce any variation of the traveltime due to ray bending, so that any change in the traveltime is likely to be due to the effects of anisotropic wave propagation. Thus the anisotropic shear-wavefield is parametrized in terms of the $qS1$-wave polarization azimuth in the horizontal plane and the $qS2 - qS1$ time-delay. The measured observations are shown in Figs 6 and 7a with an estimated error envelope given by Queen and Rizer (1990) for the time-delays. Using these values we set $\delta\tau_i$ to be a constant 4 ms for $qS2 - qS1$ time-delays and δp_i to be 15" for the $qS1$-wave polarizations.

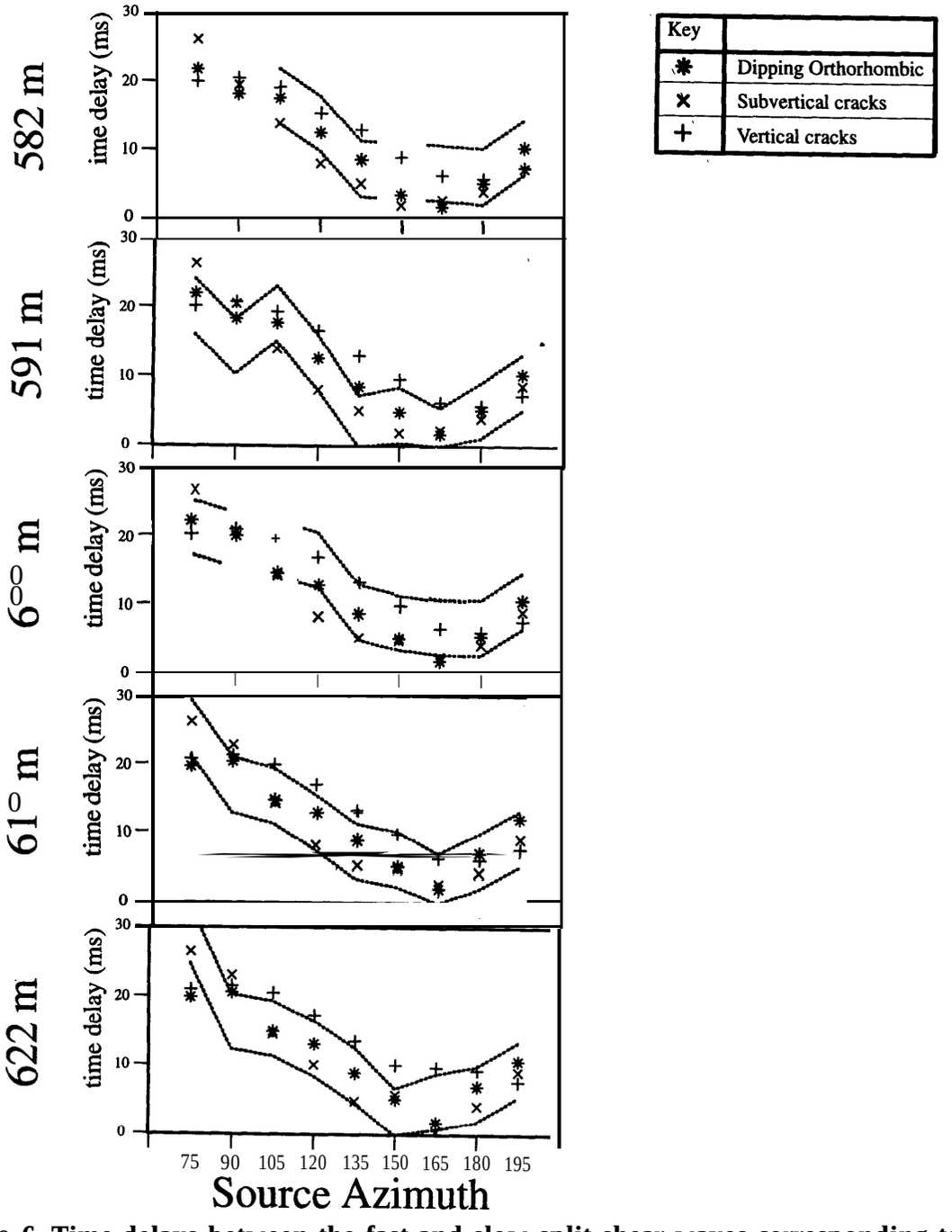

Figure **6. Time-delays between the fast and slow split shear waves corresponding to the optimal models found by the GA for different** parametrizations. **The dashed lines indicate' the upper and lower estimated error bounds for the observed time-delays. Breaks in the dashed lines indicate that no data was available.**

Inversion of field data from the azimuthal VSP

Inversions were attempted with several anisotropic symmetry systems. These results are summarized in Table 1 and Figs 6, 7b, c and d.

The simplest anisotropic model used in the inversion is a TIH system. Although the time-delays can be adequately explained in terms of such a system, the

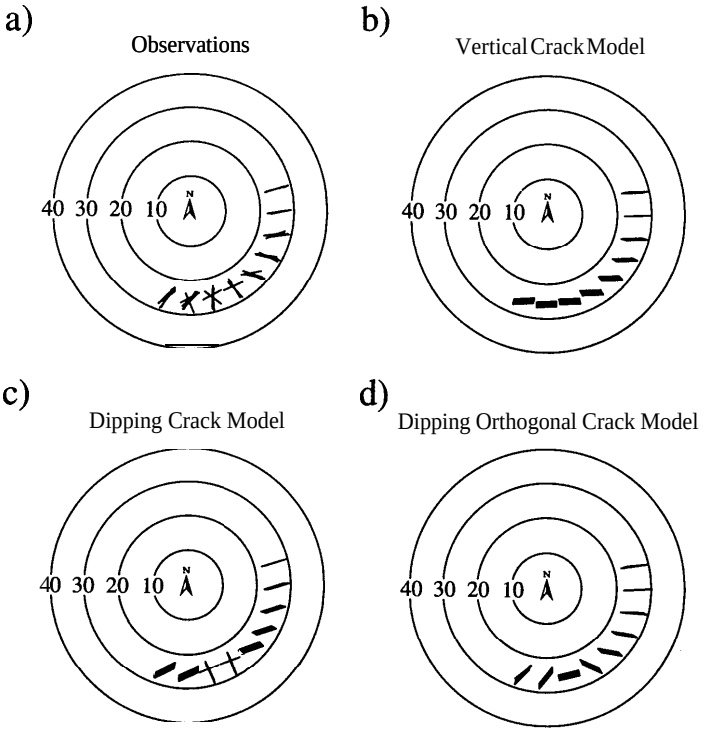

Figure **7. Polarization of the $qS1$-wave plotted on a lower hemisphere equal area projection corresponding to (a) the observations recorded using the AVSP geometry and (b)-(d) the optimal model observations obtained from the GA for different parametrizations. The $qS1$ polarizations are plotted for the optimal (b) vertical crack model, (c) dipping crack model and (d) dipping orthogonal crack model. Each circle represents equi-incident angle propagation with the outermost representing propagation at 40" to the vertical.**

observed $qS1$-wave polarizations are inconsistent with a single vertical crack model [Queen and Rizer (1990) found that a wet crack system striking at N75°E with a crack density of 0.04 could model all but a few of the observations]. The GA inversion for the observed $qS1$-wave polarizations and time-delays using this TIH system finds a best-fit model similar to that given by Queen and Rizer (1990) with wet cracks striking at N87°E, with CD, = 0.05, AR, = 0.02 and a misfit of 3.5. This crack strike is only just within the acceptable range suggested by ***a priori*** information determined from BHTV and geological measurements. The poor estimation of the crack strike is thought to be due to the averaging of the azimuthal variation of the observed $qS1$-wave polarization estimates to give an average crack strike direction, since for a single vertical crack set there is a broad band of horizontal $qS1$-wave polarizations parallel to the crack strike. This is confirmed if the residual is decomposed into the time-delay and polarization contributions, showing that the large residual is largely due to a poor fit of the polarization observations.

The second system that could account for such azimuthal anisotropy is a dipping crack system. The symmetry class is identical to that for vertically aligned cracks but an additional degree of freedom is required to specify the orientation of the symmetry axis since it is no longer constrained to the horizontal plane. Previous studies (Queen and Rizer 1990; Liu, Crampin and Queen 1991) in the area indicate

Table 1. **Summary of the inversion results for the AVSP. The first two columns indicate the parameters included in the inversion. For 'dipping cracks' a parameter, *DIP*, was included defining the orientation of the cracks from the horizontal plane. For the orthorhombic inversion a second crack set (sub-horizontal) orthogonal to the first (sub-vertical) was included requiring an additional three crack parameters. This second set is shown on the second line in the appropriate columns. The crack and orientation parameters shown are those corresponding to the optimal model found by the GA with the corresponding misfit value shown in the last column. *AZI* is measured in degrees from north in a clockwise direction.**

	OPTIMAL MODEL										
	Hudson Cracks			Orientation		Elastic Constants					
	CD	*AR*	*CT*	*AZI*	*DIP*	C_{11}	C_{22}	C_{44}	C_{55}	C_{12}	misfit
Vertical cracks	**0.05**	**0.02**	**w**	**87.0**	n/a	**30.41**	**31.60**	**8.00**	**7.19**	**15.21**	**3.5**
Dipping cracks	**0.06**	**0.07**	**w**	**69.0**	**10.0**	**27.43**	**30.86**	**8.00**	**7.04**	**13.72**	**1.8**
Orthorhombic	**(0.03**	**0.12**	**d**	**75.0**	**7.0**						**1.4**
	0.04	**0.01**	**w)**								

that dipping fractures are present at shallow depths rotated 20” from the vertical to the south-east. Evidence from dipmeter and BHTV measurements also suggest the presence of dipping fractures. So in the second inversion a parameter is included specifying the dip of the cracks from the vertical axis, spanning a range from $+32°$ to $-32°$. The remaining crack parameters were identical to those used for the vertical crack inversion described above. The best-fit model obtained from this inversion was a wet crack model with cracks striking at N69°E and rotated 10” from the vertical to the south-east with CD_1 = 0.06 and AR, = 0.07. The residual value for this model was almost half that obtained for the vertical crack set.

There are several interesting points to note from this inversion. Firstly, the introduction of crack dip allows an estimation of the crack strike which is more consistent with the ***a priori*** information. Secondly, the abrupt swings in the $qS1$-wave polarizations observed at azimuths 6 through to 8 are reproduced in the crack model as can be seen on examining Fig. 7c. These polarization swings in the optimal crack model observation set are due to the presence of a line singularity.

The next lowest symmetry class to be inverted, after hexagonal, is orthorhombic, which can be represented as two orthogonally intersecting crack sets. For the orthorhombic inversion, three additional horizontal crack parameters were included describing the second orthogonal horizontal crack set. As before the first crack set is initially restricted to be vertical. As before the resulting system was then rotated by the AZI and DIP parameters. Results from the inversion gave a best-fit model with a misfit of 1.4 and crack parameters as indicated in Table 1. The orientation of the symmetry axis is consistent with previous versions and indicates a crack strike of N75°E rotated by 7” from the vertical to the south-east. The decrease in the misfit function is not surprising since horizontal cracks introduce. three additional degrees of freedom. It is not then surprising that an orthorhombic system simulated by two dipping intersecting orthogonal crack sets gives the lowest overall misfit of 1.3.

Although Queen and Rizer (1990) suggested the presence of two non-orthogonal crack sets as a possible explanation for the results obtained from the AVSP based on other observations, there is insufficient azimuthal coverage to warrant further inversions with even lower symmetries.

Experimental configuration for azimuthal RVSP (AR VSP)

Reverse vertical seismic profiles (RVSP) have also been shot at the CBTF, centred around a shallow borehole GW3 located approximately 135 m to the south of well 33-l. The experimental configuration is shown in Fig. 8. Ten three-component surface geophones were located on an arc of radius 7.2 m extending from N358°E to N160°E with an azimuthal spacing of approximately 18°. The Conoco rotary downhole source was used to generate horizontally and vertically polarized shear waves at depths between 1.5 and 38.4 m at intervals of approximately 0.6 m. Shear-wave polarizations corresponding to sources located at 10, 15 and 25 m were used

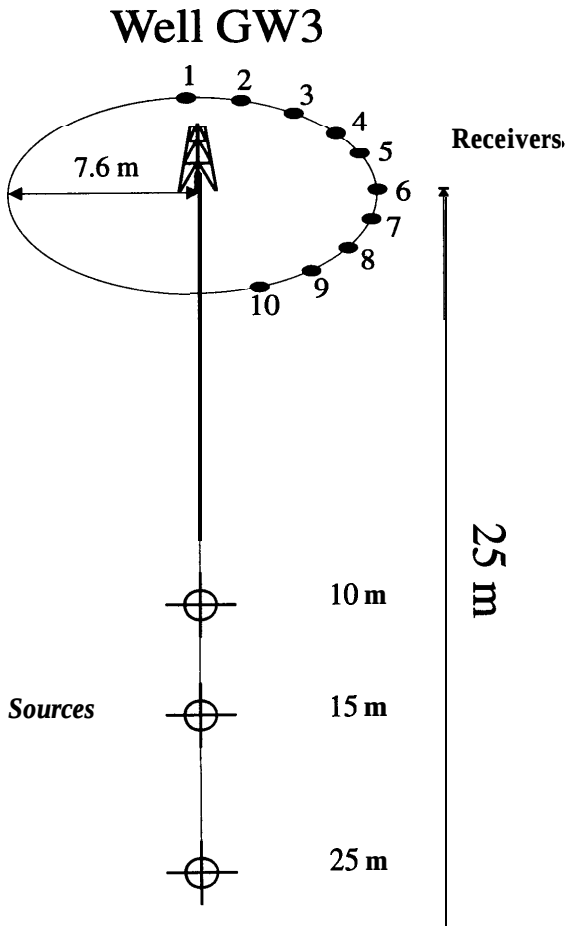

Figure 8. **Schematic illustration of the acquisition geometry used for the azimuthal RVSP showing the Conoco rotary source and three-component surface geophone positions, shown as crossed circles and filled circles, respectively.**

in the inversion providing a more extensive coverage of incident angles than that given by the AVSP. Time-delays were not inverted as the estimates were scattered and thought to be unreliable (Liu, personal communication). The polarization estimates have been published previously by Liu, Crampin and Queen (1991).

Inversion of field data for azimuthal RVSP

As for the AVSP, several inversions were carried out with different anisotropic symmetries as summarized in Table 2 and Fig. 9.

The first entry in Table 2 describes the results using a simple vertical crack system. The inversion results indicate a highly anisotropic region of crack density 0.10 with wet cracks striking at N81°E, although the crack density is unlikely to be well resolved with the absence of time-delay observation estimates. As with the vertical crack inversion for the AVSP, the orientation of the crack set is only just within the acceptable bounds given by ***a priori*** information. There is a considerable difference in the inverted CDs for the ARVSI? and the AVSP which is not unexpected since the ARVSI? extends over a shallow depth range of only 50 m where

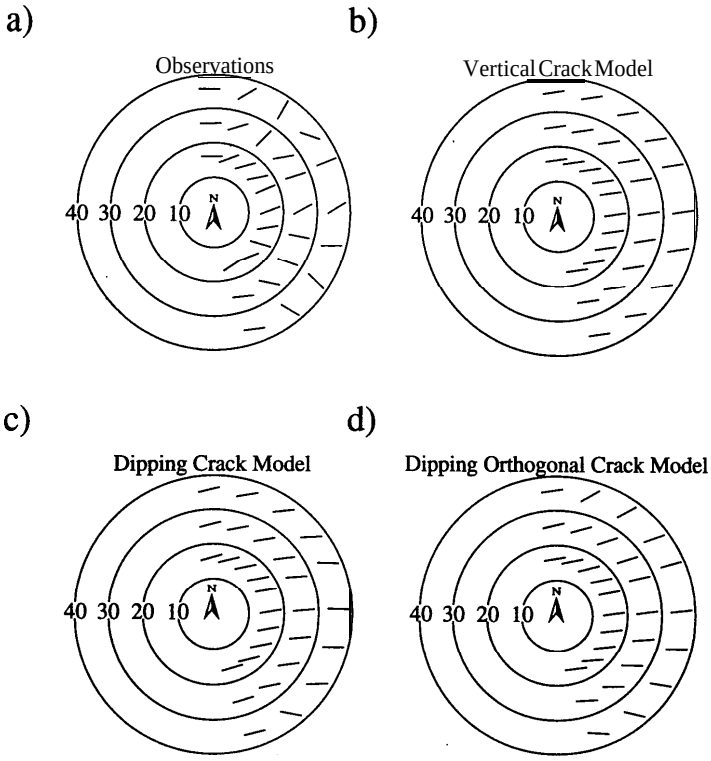

Figure 9. **Polarization of the $qS1$ shear wave plotted on an upper hemisphere equal area projection corresponding to (a) the observations recorded using the ARVSP geometry and (b)-(d) the optimal model observations obtained from the GA for different parametrizations. The $qS1$ polarizations are plotted for the optimal (b) vertical crack model, (c) dipping crack model and (d) dipping orthogonal crack model. Each circle represents equi-incident angle propagation with the outermost representing propagation at 40" to the vertical.**

high crack densities may be expected in **the near surface.** Liu, Crampin and Queen (1991) found that the ARVSP results could be adequately modelled using a CD, of 0.12 which is similar to the CD, obtained by the inversion.

The inversion results for the dipping crack system suggest dry cracks striking N76°E and rotated 26" from the vertical to the south-east. This result agrees almost exactly with that obtained by Liu, Crampin and Queen (1991), who modelled the ARVSP using a crack set striking at N75°E and rotated 20" from the vertical to the south-east.

Synthetic modelling for the A VSP

Based on the results obtained from the GA inversion, full waveform modelling was attempted for the AVSP. The isotropic velocity structure at the CBTF was modelled using 17 layers and a lower half-space with velocities and densities based on logs from well **33- 1.**

The purpose of this modelling was to verify the results obtained from the inversion and to examine the effect of replacing the homogeneous half-space used in the

Table **2. Summary of the inversion results for the ARVSP. The format of this table follows that of Table 1.**

	OPTIMAL MODEL										
	Hudson Cracks			Orientation		Elastic Constants					
	CD	*AR*	*CT*	*AZI*	*DIP*	C_{11}	C_{22}	C_{44}	C_{55}	C_{12}	misfit
Vertical cracks	**0.10**	**0.13**	**w**	**81.3**	n/a	**22.78**	**29.69**	**8.00**	**6.46**	**11.39**	**2.2**
Dipping cracks	**0.08**	**0.11**	**d**	**75.5**	**25.9**	**20.01**	**29.00**	**8.00**	**6.74**	**10.01**	**2.0**
Orthorhombic	**(0.07**	**0.10**	**d**	**81.3**	**0.5**						**1.3**
	0.13	**0.09**	**w)**								

GA forward modelling step with a depth-dependent velocity structure. The synthetic seismograms produced were analysed by application of the same automatic techniques with the same time windows as had been used to extract the shear-wave attributes from the field data.

Synthetic seismograms were generated using the ANISEIS (Taylor 1990) modelling package which generates full-wave seismograms using the reflectivity method. The multi-azimuthal nature of the survey combined with propagation passing near to a line singularity required an integration over azimuthal as well as vertical slowness, so that the resulting forward modelling problem is time consuming, requiring 9 hours CPU on a VAX 4000/400 (Specmark 22.3).

The model which reproduced the observed shear-wave polarizations and time-delays most accurately was a wet crack model with cracks of AR, equal to 0.07 striking N74°E and rotated 17" from the vertical to the south-east. The predicted shear-wave polarizations and $qS2 - qS1$ time-delays for this model are plotted in Figs 10a and 1 la, respectively. In order to model the time-delays, a high CD_1 of 0.12 was required in the top 130 m of the model and below this a CD_1 of 0.065 was used. This high crack density agrees well with the GA inversion results for the ARVSP and also with full wave modelling conducted by Liu, Crampin and Queen (1991). The $qS1$-wave polarizations were found to be adequately modelled with the abrupt swings observed in the field data being reproduced in the synthetic model due to propagation through a line singularity. As expected, the position of the line singularity was extremely sensitive to the crack orientation and rotations as small as 0.25' could significantly affect the shear-wave polarizations. The discrepancy between the dip of the cracks obtained from matching full waveform synthetics and that obtained from the GA inversion is most probably due to the introduction of a laterally uniform velocity structure leading to ray bending.

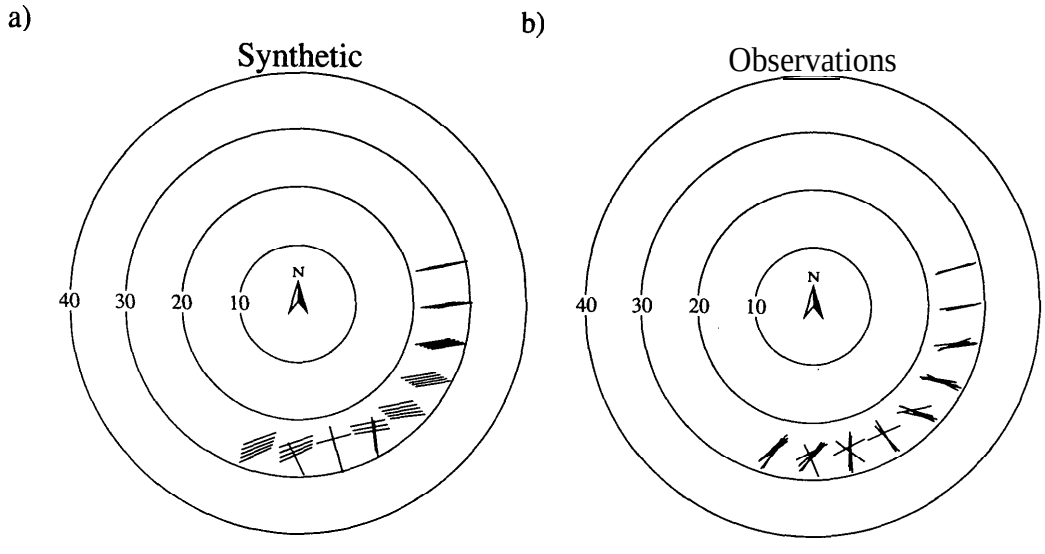

Figure 10. Polarization of the $qS1$ shear waves measured **from north for (a) the synthetic model observations and (b) the field observations plotted on a lower hemisphere** equal area **plot.**

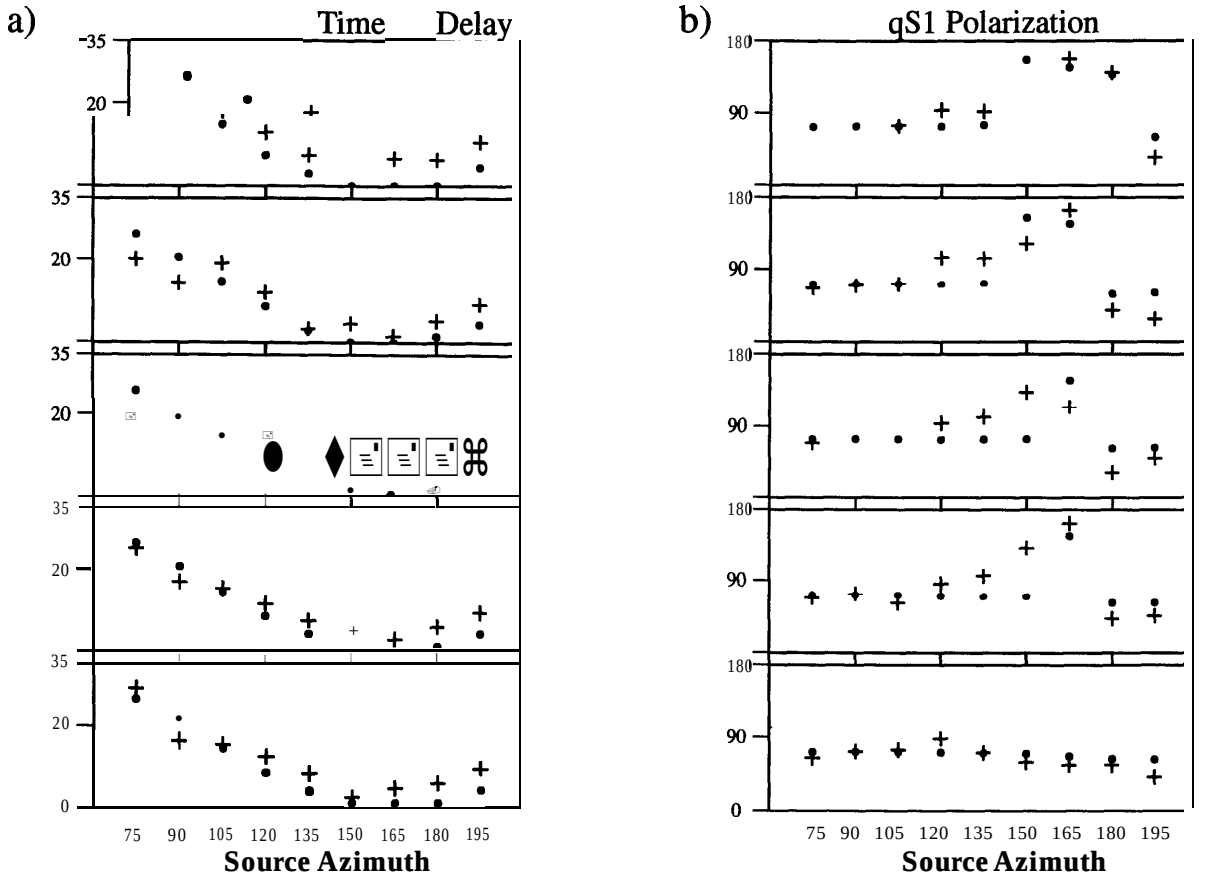

Figure 11. **Estimation results showing (a) the time-delay between the fast and slow split shear waves and (b) the $qS1$ polarization in the horizontal plane for the synthetic model observations and field observations. Results are plotted as a function of the source azimuth. Figures 10a and b show the same $qS1$ polarizations but plotted on an equal area plot.**

The final model derived by full waveform synthetics is similar to that obtained by GA inversion techniques. This similarity is encouraging, considering the relatively small CPU requirement of a GA inversion compared to the full wave modelling. However, the GA inversion should be regarded as an initial step before, rather than a substitute for, full waveform synthetic modelling.

Discussion and conclusions

The inversion results that have been presented here for both the AVSP and the ARVSP have been found to be consistent with previous geological and numerical studies of the observed shear-wave anisotropy. In both cases the results appear to suggest that the presence of dipping fractures at the CBTF can be detected from the horizontal projections of the shear-wave polarizations from offset VSP data. The disturbance in the shear-wave polarizations measured at azimuths 6 to 8 with the AVSP was found to be modelled by using a line singularity. To identify the line singularity positively, it would be necessary to choose a field geometry that

would cross the line singularity where an abrupt change in shear-wave polarizations and zero time-delays would be observed.

The most significant problem with this work is the simplification of the forward modelling from what is in reality a 3D structure to an anisotropic homogeneous half-space. This approach is justified firstly by the prohibitive computational complexity and intensity of the forward modelling requirements that would be required in dealing with a more realistic anisotropic earth model. Secondly, it is unlikely that there are any significant changes in the crack orientation with depth (although there may be some rotation of crack direction to the vertical with depth due to the increase in the overburden) so that the polarizations measured at the geophones will correspond to the local anisotropy. Problems arise for the inversion of the time-delays since these are proportional to the shear-wave velocity which are not constant with depth. In this case the inverted time-delays will effectively average the shear-wave velocities sampled along the raypaths. Since time-delays are also proportional to the crack density, the inversion result will refer to a weighted average crack density over the region. Despite these limitations the GA appears to produce consistent results so that it would appear that these assumptions are valid. It should be emphasized that these limitations are related to the computational complexity of the forward modelling problem and not the nature of the inverse problem structure for the GA.

As with previous studies (Stoffa and Sen 1991; Sambridge and Drijkoningen 1992), the GA has been found to perform very efficiently when applied to the search of large non-linear model spaces. The main limitation with the GA is the dependence on the speed with which the fitness functions can be evaluated since many models need to be generated before convergence. However, for large multimodal model spaces where the implementation of a Monte-Carlo process is considered impractical due to the slow convergence rate, the GA presents an attractive alternative. GAs are also very flexible and may be applied to different problem domains by replacing the evaluation routine by the relevant forward modelling problem. More fundamental problems exist with GAs but it appears that in most cases these schemes are robust and efficient and are likely to find increasing use within the exploration industry.

We have shown that an inversion scheme based on a GA can be used to invert shear-wave observations in the presence of seismic anisotropy and in future studies we intend to extend the GA approach to the inversion of guided wave dispersion in anisotropic waveguides.

Acknowledgements

S. Horne thanks Elf UK for their financial support of this work and also colleagues at the British Geological Survey for their support, advice and friendship. This work was supported by the Edinburgh Anisotropy Project and the Natural

Environment Research Council, and is published with the approval of the Director of the British Geological Survey (NERC).

References

Alford R.M. 1986. Shear data in the presence of azimuthal anisotropy: Dilley, Texas. 56th SEG meeting, Houston, Expanded Abstracts, 476-479.

Arts R. J., Helbig K. and Rasolofosaon P.N. J. 1991. Complete inversion of the anisotropic elastic tensor in rocks: Experiment and theory. 61st SEG meeting, Houston, Expanded Abstracts, 1538-l 541.

Backus G.E. 1962. Long-wave elastic anisotropy produced by horizontal layering. *Journal of Geophysical Research* 66, 4427–4440.

Chapman C.H. and Pratt R.G. 1992. Traveltime tomography in anisotropic media – I. Theory. *Geophysical Journal International 109,* 1 – 19.

Crampin S. 1985. Evaluation of anisotropy by shear-wave splitting. *Geophysics* 50, 42–1 52.

Crampin S. 1987. Geological and industrial implications of extensive-dilatancy anisotropy. *Nature* 328, 491–496.

Douma J. 1988. The effect of the aspect ratio on crack-induced anisotropy. *Geophysical Prospecting* 36, 614–632.

Folstad P.G. and Schoenberg M. 1993. Scattering from a set of anisotropic layers to second order in frequency. 55th EAEG meeting, Stavanger, Norway, Expanded Abstracts, p. 105.

Goldberg D.E. 1898. *Genetic Algorithms in Search Optimization and Machine Learning.* Addison-Wesley Pub. Co.

Hudson J.A. 1986. A higher order approximation to the wave propagation constants for a cracked solid. *Geophysical Journal of the Royal astronomical Society* 87, 265–274.

Hudson J.A., 1991. Crack distributions which account for a given seismic anisotropy. Geo*physical Journal International 104, 5 17-52* 1.

Li X.Y. and Crampin S. 1993. Linear-transform techniques for processing shear-wave anisotropy in four-component seismic data. *Geophysics 58,* 240–256.

Liu E. and Crampin S. 1990. Effects of the internal shear-wave window: comparison with anisotropy induced splitting. *Journal of Geophysical Research 95,* 11275-l 1281.

Liu E., Crampin S. and Queen J.H. 1991. Fracture detection using cross-hole surveys and reverse vertical seismic profiles at the Conoco Borehole Test Facility, Oklahoma. *Geophysical Journal International* 107, 449–463.

MacBeth C. 1991. Inverting shear-wave polarizations for anisotropy using three component offset VSP's : synthetic seismograms. *Geophysical Journal International* 107, 571-583.

Musgrave M. J. 1970. *Crystal Acoustics.* Holden-Day Inc.

Queen J.H. and Rizer W.D. 1990. An integrated study of seismic anisotropy and the natural fracture system at the Conoco Borehole Test Facility, Kay County, Oklahoma. *Journal of Geophysical Research 95, 11255-l 1273.*

Sambridge M. and Drijkoningen G. 1992. Genetic algorithms in seismic waveform inversion. *Geophysical Journal International 109, 323-342.*

Smith M.L., Scales J.A. and Fischer T.L. 1992. Global search and genetic algorithms. *The Leading Edge of Exploration* 11, *22-26.*

Stoffa P.L. and Sen M.K. 1991. Nonlinear multiparameter optimization using genetic algorithms : inversion of plane wave seismograms. *Geophysics* 56, 1794-1810.

Tatham R.B. and McCormack M.D. 1991. Multicomponent seismology in petroleum exploration. In: *Investigations in Geophysics,* No. 6. (eds). E.B. Neitzel and D.F. Winterstein SEG.

Taylor D.B. 1990. ANISEIS manual : version 4.5 : Applied Geophysical Software Inc., Houston.

Thomsen L. 1986. Weak elastic anisotropy. *Geophysics* 51, 1954 – 1966.

Zeng X. and MacBeth C. 1993. Algebraic processing techniques theory. *Geophysical Prospecting* 41, 1033 – 1066.